ADVANCED MATERIALS TECHNOLOGIES
www.advmattechnol.de

Machine Learning-Based Solution for Thermomechanical Analysis of MMIC Packaging

Sumin Kang, Jae Hak Lee, Seung Man Kim, Jaeseung Lim, Ah-Young Park, Seongheum Han, Jun-Yeob Song, and Seong-Il Kim*

Thermomechanical analysis of monolithic microwave integrated circuit (MMIC) packaging is essential to guarantee the reliability of radio frequency/microwave applications. However, a method for fast and accurate analysis of MMIC packaging structures has not been developed. Here, a machine learning (ML)-based solution for thermomechanical analysis of MMIC packaging is demonstrated. This ML-based solution analyzes temperature and thermal stresses considering key design parameters, including material properties, geometric characteristics, and thermal boundary conditions. Finite element simulation with the Monte Carlo method is utilized to prepare a large dataset for supervised learning and validation of the ML solution, and a laser-assisted thermal experiment is conducted to verify the accuracy of the simulation. After data preparation, regression tree ensemble and artificial neural network (ANN) learning models are investigated. The results show that the ANN model accurately predicts the outcomes with extremely low computing time by analyzing the high-dimensional dataset. Finally, the developed ML solution is deployed as a web application format for facile approaches. It is believed that this study will provide a guideline for developing ML-based solutions in chip packaging design technology.

1. Introduction

Monolithic microwave integrated circuits (MMICs) have led to rapid advances in radio frequency (RF) applications, including 5G base stations, automotive radar, and satellite communication systems.[1–4] In this regard, a packaging strategy considering temperature and thermal stresses is key to ensuring the reliability of the MMICs because the large amount of heat generated by the high power density and small form factor often causes thermomechanical failure.[5–9] An MMIC packaging structure involves many design parameters, such as material selection for each part, geometric characteristics, and thermal boundary conditions (BCs). In this context, obtaining analytical or empirical solutions to analyze the MMIC packaging structure is a formidable task owing to the nonlinearly correlated and high-dimensional design parameters. Multiphysics finite element method (FEM) simulation can provide accurate prediction results for the MMIC packaging structure.[10–13] However, additional FEM simulations have to be conducted whenever the design parameters are changed, resulting in high computing costs and time-consuming processes. Therefore, a facile, fast, and accurate solution for thermomechanical analysis of the MMIC packaging problem is required.

A machine learning (ML) framework has recently been utilized to analyze various engineering problems, including cardiovascular organs,[14–16] cantilevered structures,[17,18] and composite materials.[19,20] In particular, the ML framework allows the prediction of critical reliability parameters in chip package structures, such as energy release rates,[21] warpage behaviors,[22] and drop responses.[23] Furthermore, several studies have presented analysis models for the accelerated reliability of solder joints under thermal cycling conditions using artificial neural network (ANN) architectures.[24–26] These ML approaches driven by FEM simulation data have been regarded as a fast and accurate surrogate of the simulation. However, despite these successful efforts, an ML-based analysis for MMIC packaging concerns has not yet been developed.

In this study, we present an ML-based solution for thermomechanical analysis of MMIC packaging. The ML solution is designed to analyze the maximum values of temperature and

S. Kang, J. H. Lee, S. M. Kim, A.-Y. Park, S. Han, J.-Y. Song
Department of Ultra-Precision Machines and Systems
Korea Institute of Machinery and Materials (KIMM)
Daejeon 34103, Republic of Korea
E-mail: suminkang@kimm.re.kr
J. Lim
School of Mechanical Engineering
Chonnam National University
Gwangju 61186, Republic of Korea
S.-I. Kim
Defense Materials and Components (DMC) Convergence Research Department
Electronics and Telecommunications Research Institute (ETRI)
Daejeon 34129, Republic of Korea
The ORCID identification number(s) for the author(s) of this article can be found under https://doi.org/10.1002/admt.202201479.

DOI: 10.1002/admt.202201479

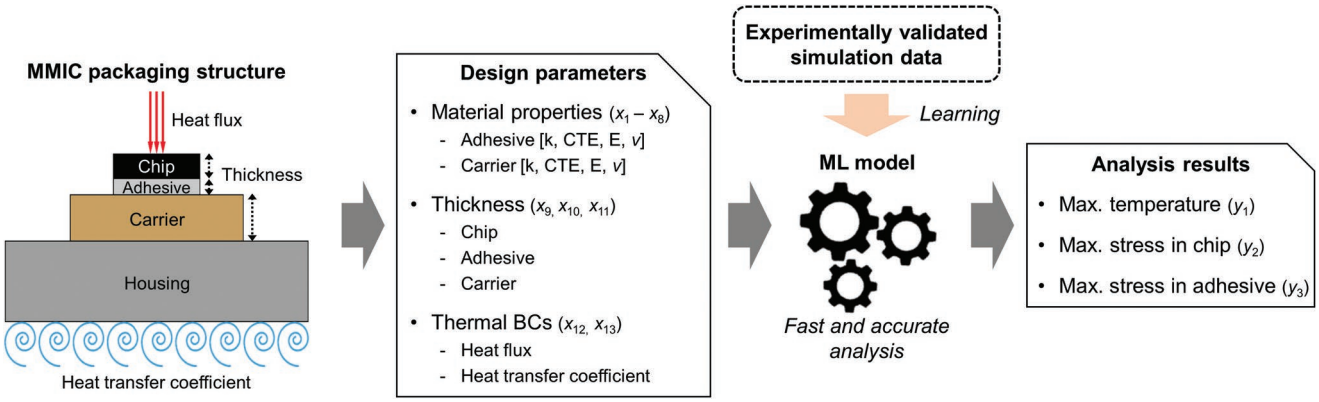

Figure 1. ML-based solution for fast and accurate analysis of MMIC packaging.

thermal stresses of chip–adhesive–carrier–housing packaging structures considering 13 design parameters categorized into materials properties, geometric characteristics, and thermal BCs. FEM simulation with the Monte Carlo method was conducted to prepare 40 000 data samples, and a laser-assisted thermal experiment was performed to verify the simulation results. The prepared datasets were utilized for the supervised learning and validation of various ML models, including regression tree ensemble and ANN models. Moreover, the minimum errors of each ML model were investigated by optimizing their hyperparameters. Finally, we deployed the developed ML solution as a web application format for facile approaches for general users.

2. Results and Discussion

2.1. Outline of the ML-Based Solution for the MMIC Packaging Problem

Figure 1 outlines the ML-based fast and accurate analysis solution for MMIC packaging structures. The ML solution was designed to provide thermomechanical analysis results when several design parameters were input into the ML model, which was constructed based on experimentally validated simulation data. In this regard, 13 design parameters related to material properties, layer thickness, and thermal BCs were defined considering the traditional gallium-nitride (GaN)-based MMIC packaging structure composed of chip–adhesive–carrier–housing.[27] In the structure, 4H-silicon carbide (SiC) and Al6061 alloy were used as the chip and housing materials, respectively, because GaN transistors are typically produced on high-quality 4H-SiC chips, and the low density of Al6061 is advantageous for reducing weight.[28,29] In contrast, many suitable candidates for the adhesive and carrier materials were available.[7,27,30] Accordingly, the material properties of the adhesive and carrier (thermal conductivity, coefficient of thermal expansion (CTE), elastic modulus, and Poisson's ratio) were regarded as the input variables (x_1–x_8). Moreover, the thicknesses of the chip, adhesive, and carrier layers were adjustable input variables (x_9, x_{10}, and x_{11}), which can influence heat transfer performance and thermal deformation behaviors.[31,32] Finally, a surface heat flux was applied to a local region on the top surface of the chip, and convection cooling was applied to the bottom surface of the housing. Here, the surface heat flux reflects thermally dissipated power from the GaN-based electronic circuits placed on the top surface of the SiC chip.[27,33,34] The thermal BCs (surface heat flux and heat transfer coefficient) were regarded as important variables in the MMIC packaging design (x_{12} and x_{13}).

The output analysis results were defined as the maximum values of temperature in the MMIC package structure (y_1), principal stress in the chip (y_2), and von Mises stress in the adhesive (y_3). These output variables are critical indicators for predicting failure behaviors of the MMICs. The MMIC devices require qualified operating and storage temperatures due to thermal degradation.[35] Moreover, thermal stresses in the MMIC structure are caused by CTE mismatch and warpage behavior, often resulting in failures of the chip and adhesive parts. Despite the high fracture strength of 4H-SiC,[36] the thermal stress in the chip causes chip cracking due to the presence of material defects such as microcracks, scratches on the surface, and chipping on the edges.[37–39] In addition, cracking or delamination behaviors in the adhesive are frequently caused by the stress concentration effect.[40,41]

2.2. FEM Simulation for Data Preparation and Its Experimental Validation

After defining the input and output variables, FEM simulation was performed to prepare a large dataset for supervised learning. **Figure 2**a shows a 3D model of the chip–adhesive–carrier–housing MMIC packaging structure. In this model, 4H-SiC and Al6061 were assigned for the chip and housing, respectively, and the material properties of the adhesive and carrier were changed based on the selection of materials. The assigned material properties are represented in Table S1 (Supporting Information). The in-plane dimensions of the chip, adhesive, and carrier were fixed at 5×5, 5×5, and 11×14 mm^2, respectively, and the housing had a constant dimension of $50 \times 50 \times 10$ mm^3. The layer thicknesses varied in the ranges of 30–200 μm, 10–100 μm, and 0.3–2.5 mm for the chip (x_9), adhesive (x_{10}), and carrier (x_{11}), respectively. Furthermore, the surface heat flux (x_{12}) was changed in the range of 1–30 W, and the heat transfer coefficient (x_{13}) in that of 0–300 W m^{-2} K^{-1}. Detailed information on the FEM simulation is described in

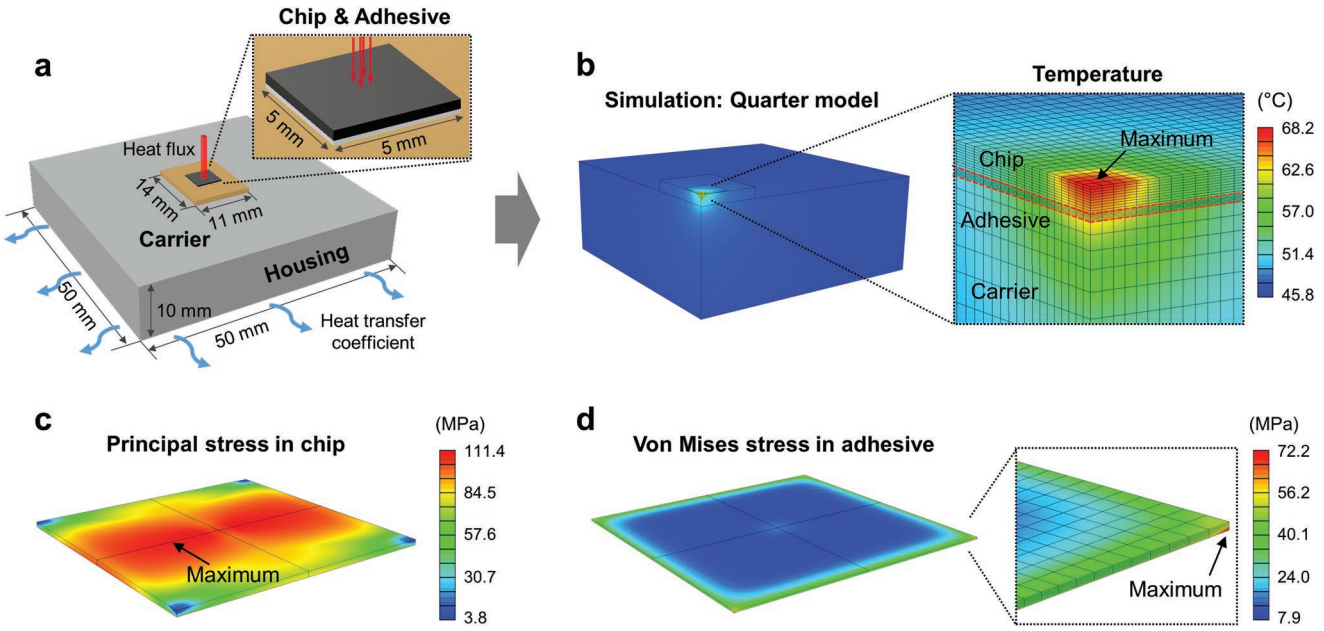

Figure 2. Simulation modeling and representative results. a) 3D full model of MMIC packaging structure. b) 3D quarter model in the simulation and its temperature profile. c) Principal stress distribution in the chip. d) Von Mises stress distribution in the adhesive.

the Experimental Section. Consequently, 40 000 samples of a dataset were prepared by randomly assigning input values within the defined ranges for each variable and obtaining the corresponding output values with the FEM simulation. The whole dataset was generated in ≈28 days because the average computing time for each simulation was 60 s when running in parallel on 16 CPUs. The prepared dataset is presented in Table S2 (Supporting Information).

Figure 2b shows a 3D quarter simulation model of the MMIC packaging structure and its temperature distribution. The quarter model in the simulation was suitable owing to the *x*- and *y*-axis symmetry conditions, which significantly reduced the calculation time. The enlarged view in Figure 2b indicates that the maximum temperature was located at the center of the heat source region, and the temperature decreased gradually as the distance from the center point increased (Figure S1, Supporting Information). Figure 2c,d depicts the distribution of thermal stresses in the chip and adhesive. The maximum principal stress, a representative failure criterion of brittle materials, was located inside the chip. The maximum von Mises stress was located at the edge of the adhesive, indicating the potential for interfacial delamination due to peeling moments.[42]

To verify the accuracy of the simulation data, we conceived a laser-assisted thermal testing method (**Figure 3**a). In the experiment, the center point of the top surface of the MMIC chip was irradiated for 15 min with a 532 nm continuous-wave laser beam with 2.5 W input power, and a thermal imaging camera measured the maximum temperature. MMIC packaging specimens which were composed of 4H-SiC chip-sintered Ag

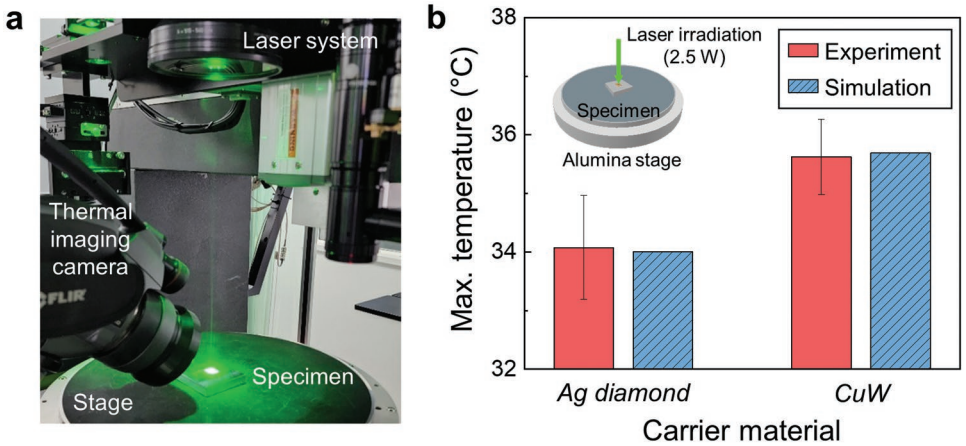

Figure 3. Experimental validation of the simulation results. a) Experimental setup for measuring the maximum temperature of the MMIC packaging structure. b) Maximum temperature of the MMIC packaging structures for two different carrier materials, Ag diamond and CuW.

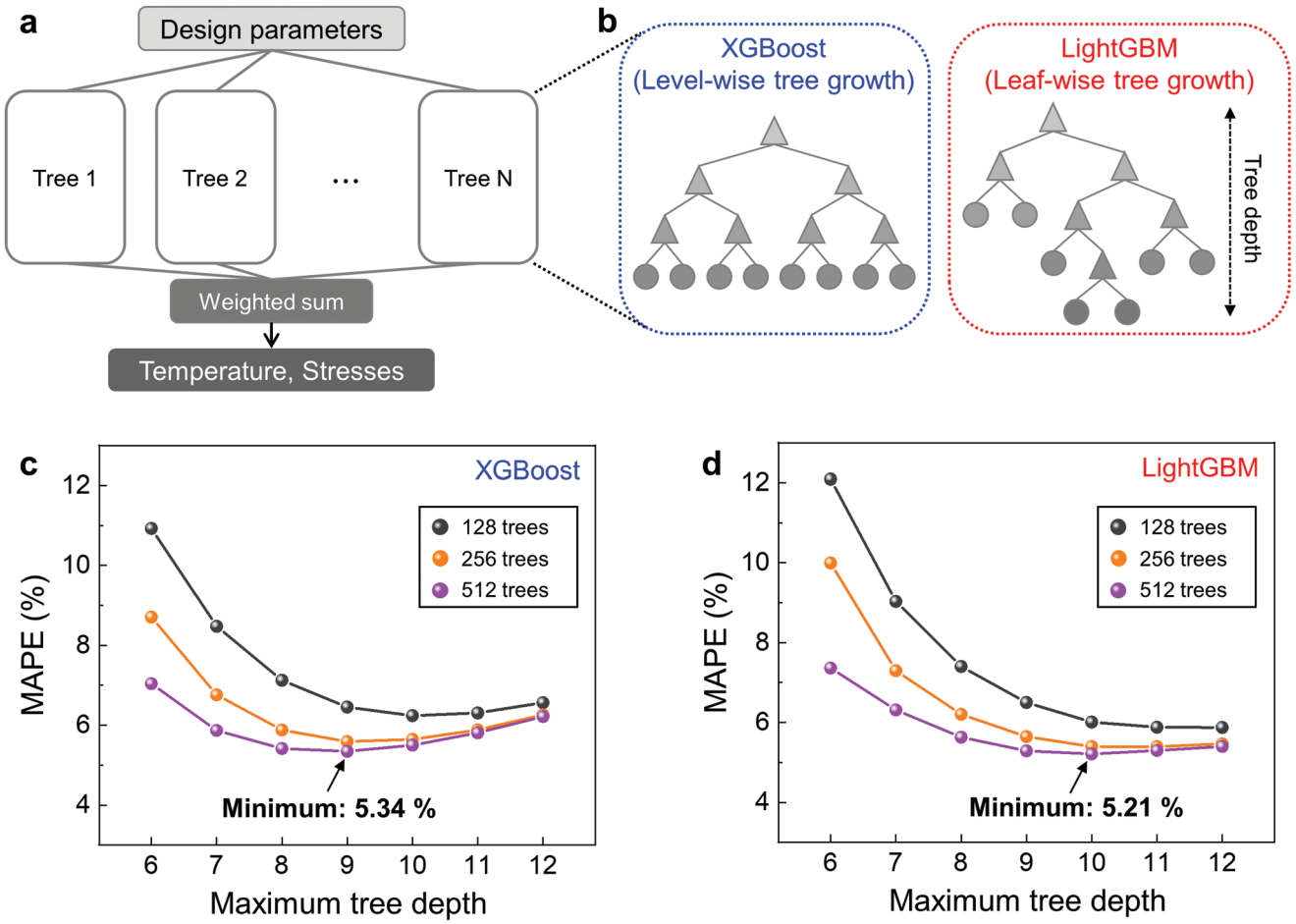

Figure 4. Results of regression tree ensemble models. a) Schematic of a regression tree ensemble structure composed of a set of weak regression trees. The ensemble structure predicts the results by aggregating responses from each regression tree. b) Two different tree growth strategies denoted as level-wise tree growth for XGBoost and leaf-wise tree growth for LightGBM. c,d) Prediction results of the XGBoost and LightGBM models with respect to the number of trees and tree depth.

adhesive–carrier–Al 6061 housing structures, were tested with respect to two types of carrier materials, Ag diamond and CuW. The specimens were placed on an x–γ–θ controllable alumina stage that acted as a heat spreader by dissipating accumulated thermal energy from the packaging structure. Accordingly, the experiment and simulation were compared by reflecting the effect of the alumina stage in the FEM simulation model (Figure S2, Supporting Information). The results show that the maximum temperature values obtained in the simulation agreed well with the experiment, thereby verifying the accuracy of the simulation data (Figure 3b). Furthermore, it was observed that the Ag diamond carrier, which has a high thermal conductivity of 700 W m^{-1} K^{-1}, enabled a reduction in the maximum temperature compared to that of the CuW carrier owing to the enhanced heat transfer performance.[30]

2.3. Development of the ML Solution

The prepared simulation dataset of 40 000 samples was divided into an 80% training dataset for supervised learning of the ML model and a 20% validation dataset for evaluating the accuracy of the ML model. Furthermore, regression tree ensemble and ANN models were utilized to find the best prediction model for the MMIC packaging analysis. The regression tree ensemble model is composed of a cluster of regression trees that provides more accurate results by synthesizing the responses from each tree (**Figure 4**a). In particular, we focused on the two gradient boosting models, eXtreme Gradient Boosting (XGBoost) and Light Gradient Boosting Machine (LightGBM), which are regarded as scalable, flexible, and versatile tools owing to their regularization technique.[43] The main difference between XGBoost and LightGBM is the growth strategies of each tree (Figure 4b). The trees in XGBoost are grown by splitting all nodes on the same layer simultaneously. In contrast, the trees in LightGBM are grown by expanding nodes in best-first order instead of a fixed order, allowing high computational efficiency.[44,45]

To investigate the optimum prediction performance of the regression tree ensemble models, two hyperparameters, the number of trees and maximum tree depth, were controlled. The number of combining trees in the ensemble models was

set at 128, 256, and 512, and the tree depth (i.e., the maximum number of edges from the root node to the leaf node as shown in Figure 4b) was controlled in the range of 6–12. Detailed information on the regression tree ensemble models is described in the Experimental Section. The evaluation index for the accuracy of the solution was determined as the mean absolute percentage error (MAPE) as follows

$$\mathrm{MAPE} = \frac{100\%}{3}\sum_{i=1}^{3}\left|\frac{y_i - \hat{y}_i}{y_i}\right| \quad (1)$$

where y_i is an actual value of the simulation and $\hat{y}_i$ is a predicted value obtained from the ML solution. The MAPE values were obtained by training each ML model five times with different dataset split conditions and averaging the results.

Figure 4c,d shows the results evaluated based on the validation dataset of the XGBoost and LightGBM models, respectively. The results for the training dataset are represented in Figure S3 (Supporting Information). It was found that the ensemble models with 512 trees predicted the results more accurately than those with the 128 and 256 ensemble trees, and there were optimum values of the tree depth in a moderate range. In contrast, the errors of the training dataset decreased gradually as the tree depth increased, indicating the presence of overfitting in the deep tree models. The minimum validation errors of the two models were similar: 5.34% for XGBoost and 5.21% for LightGBM. Meanwhile, owing to the efficient growth strategies, the training time of the LightGBM model was approximately six times faster than that of the XGBoost model. These results indicate that the LightGBM model is advantageous compared to the XGBoost model for the MMIC packaging analysis. However, despite their very fast training time, the prediction accuracies of regression tree ensemble models were deemed insufficient to utilize as an accurate surrogate of the simulation for the MMIC packaging problem.

Meanwhile, the ANN models, inspired by biological neural systems, have great potential for accurate prediction of outcomes considering complex nonlinearities in a dataset.[46,47] The typical structure of fully connected ANN models comprises the input layer, hidden layers, and output layer (**Figure 5**a). In this context, the number of nodes in the input and output layers was fixed at 13 and three, corresponding to the number of input and output variables, respectively. In contrast, the number of hidden layers and the number of nodes in each hidden layer are controllable and can significantly influence the prediction results. Therefore, we investigated the prediction accuracies of the ANN models by changing the number of hidden layers in the range of 1–7 and the number of nodes in that of 16–512. Detailed information on the ANN models is described in the Experimental Section.

The 3D graph in Figure 5b shows the validation errors of each ANN structure. The shallow and narrow structure of 13/16/3 showed a high error of 14.93% due to the small number of perceptrons; however, the error gradually decreased as the number of hidden layers and nodes increased. The minimum validation error of 1.69% was observed in the 13/128/128/128/128/128/3 structured ANN model, and the error slightly increased in more complex structures. Moreover, there was no remarkable difference between training and validation errors of the ANN structures (Figure S4, Supporting Information). Accordingly, we carefully anticipate that the error of the ANN models converges without overfitting issues. Based on these investigations, it can be concluded that the ANN models exhibited superior prediction performance compared with those of the regression tree ensemble models, showing a 1.69% minimum error. Further improvement of the accuracy of the ML solution can be achieved by increasing the number of training data samples (Figure S5, Supporting Information).

The best prediction results of each ML model, XGBoost, LightGBM, and ANN, were compared with the FEM simulation results (actual values), and their coefficient of determination was investigated. **Figure 6**; and Figure S6 (Supporting Information) represents the comparison results for the validation and training datasets, respectively. The optimized ML models show high conformity with the simulation results for the training dataset (Figure S6, Supporting Information), but they show a different trend in the validation dataset. In the validation dataset, even though the predicted temperature values of the three ML models were well matched with the actual values (Figure 6a), the prediction accuracy of regression tree ensemble models for the thermal stresses was insufficient compared to that of the ANN model (Figure 6b,c). In this regard, the maximum temperature is strongly influenced by the surface heat flux and heat transfer coefficient. In contrast, the thermal stresses in the chip and adhesive are determined by many input parameters including material properties, thicknesses, and

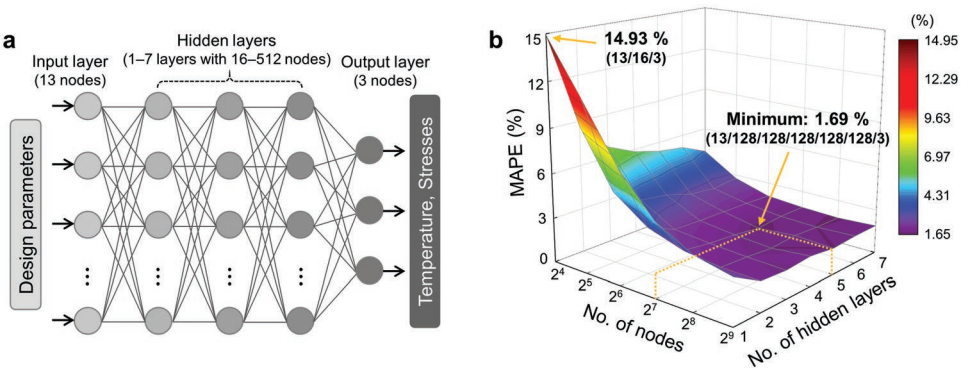

Figure 5. Results of ANN models. a) Schematic of fully connected ANN structure composed of the input layer, hidden layers, and output layer. b) The prediction results of ANN structures with respect to the number of hidden layers and nodes. The ANN structures were denoted as $n_i/n_1/n_2/.../n_k/n_o$, where n_i, n_1, n_2, n_k, and n_o are the number of nodes in the input layer, hidden layers, and output layer, respectively.

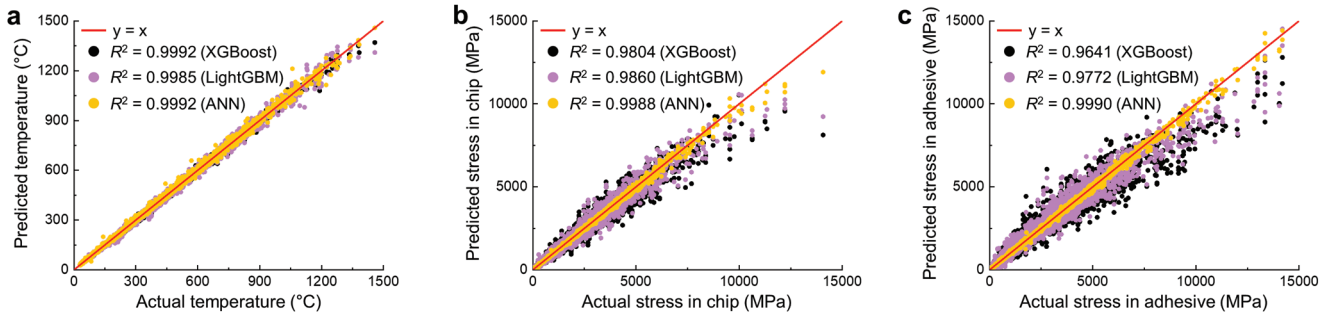

Figure 6. Comparison between ML predictions and FEM simulation results for validation dataset. The graphs comparing predicted versus actual values for three outputs: a) maximum temperature, b) maximum principal stress in chip, and c) maximum von Mises stress in adhesive. The coefficient of determination (R^2) was calculated based on the following equation: $R^2 = 1 - \sum(y_i - \hat{y}_i)^2 / \sum(y_i - \overline{y})^2$, where y_i, $\hat{y}_i$, and $\overline{y}$ are the actual value, predicted value of the ML models, and mean of the actual values, respectively.

thermal boundary conditions, showing that the thermal stresses have a high-dimensional correlation with the design parameters (Figure S7, Supporting Information). It indicates that the high accuracy of the ANN model can be attributed to the prediction capability of the high-dimensional and nonlinear dataset.

2.4. Deployment of the ML Solution

Finally, we deployed the developed ANN model as a web application format, which facilitates the use of the solution by a graphical user interface (Figure S8, (Supporting Information) https://suminkang1-mmic-packaging-web-application-wgiith.streamlitapp.com/). The distributed ML solution enables fast and accurate analysis of MMIC packaging by simply inputting several design parameters into the application, and it eliminates the need to rerun an additional FEM simulation when different conditions are applied. Especially, in terms of the computing cost of the ML solution, it produced prediction results within 0.05 s, which is significantly faster than traditional simulation analysis that consumes 30–120 s depending on the mesh elements (Figure S9, Supporting Information). The source code of the web application was shared in a public cloud to encourage users to participate in the further development of improved or new solutions for various engineering problems.

3. Conclusion

We developed an ML solution for the thermomechanical analysis of MMIC packaging using experimentally validated FEM simulation data. The ML solution was designed to output the maximum values of temperature and thermal stresses considering key input parameters related to material properties, geometric characteristics, and thermal BCs. The FEM simulation dataset was used in the training and validation of the ML model, and a laser-assisted thermal experiment was performed to verify the accuracy of the simulation data. The prediction accuracies of the regression tree ensemble and ANN models were evaluated by adjusting hyperparameters. The results indicate that the ANN model predicts the temperature and thermal stresses with a 1.69% minimum error owing to its prediction capability considering a high-dimensional and nonlinear dataset. Finally, the ML solution based on the ANN model was shared as an open-source web application to facilitate the use of the solution for many researchers.

This ML solution provided accurate thermomechanical analysis results with extremely low computing time and a simplified process, allowing fast and facile surrogate of FEM simulation. More specifically, the solution provided outcomes within 0.05 s, and the computing time of the ML solution was independent of how complex the FEM simulation models are. Furthermore, the ML solution allowed users to obtain the analysis results by simply inputting design parameters. In contrast, the conventional FEM simulation requires several steps, including modeling, defining material properties and boundary conditions, meshing, and computing. Therefore, by combining well-defined frameworks such as Bayesian optimization, the ML solution can be utilized for an efficient optimization process of the design parameters. We believe that the presented method can potentially contribute to advances in design technology by expanding to many engineering problems, not only the electronic packaging.

4. Experimental Section

FEM Simulation: Commercial software (Abaqus 6.14-3) was used for the FEM simulation. The 3D-quarter model of the chip–adhesive–carrier–housing structure was created as a deformable solid using the x- and y-axis symmetric conditions. A tie constraint of the interfaces between adjacent layers was assigned. The dissipated heat and convection cooling were assigned as the surface heat flux and heat transfer coefficient, respectively, and the initial temperature was set at 25 °C. In addition, natural convection cooling with a coefficient of 5 W m^{-2} K^{-1} was assigned to the other exposed surfaces. Regarding the boundary conditions, the *z*-axis (out-of-plane) displacement of the bottom surface of the housing was constrained, and a center point at the surface was additionally constrained with an encastre to prevent rotation and translation of the model. After modeling, a rectangular-shaped mesh with a temperature–displacement coupled type (C3D8T, an 8-node thermally coupled brick, trilinear displacement and temperature) was applied.

Regression Tree Ensemble Models: DMLC XGBoost[48] and Microsoft LightGBM[49] open-source packages were utilized for the XGBoost and LightGBM models, respectively. The learning rate and boosting type were set at 0.05 and gradient boosting tree, respectively. The upper bound

of the tree depth was controlled in the range of 6–12, and the number of weak learners with 128, 256, and 512 trees. In particular, the number of leaves in the LightGBM model was defined as $2^{(depth-1)}$, considering the characteristics of the growth strategy. The MultiOutputRegressor package was utilized to simultaneously calculate three outputs in the XGBoost and LightGBM models.

ANN Models: The ANN models were trained using the open-source platform TensorFlow.[50] Fully connected ANN models with the ReLU activation function were generated, and the Adam optimizer, mean absolute error loss function, and 5000 epochs were adopted for training the ANN models. The accuracy of the ANN models with respect to the epochs is represented in Figure S10 (Supporting Information), indicating that the models converged without overfitting. The number of hidden layers and nodes in each layer were controlled as the hyperparameters, in the ranges of 1–7 layers and 16–512 nodes.

Supporting Information

Supporting Information is available from the Wiley Online Library or from the author.

Acknowledgements

This work was supported by the Convergence Research Center Program (CRC-19-02-ETRI) of the National Research Council of Science & Technology (NST) funded by the Ministry of Science and ICT (MSIT), the Technology Innovation Program (20014846), and the Industrial Strategic Technology Development Program (1415168490) of the Korea Evaluation Institute of Industrial Technology (KEIT) funded by the Ministry of Trade, Industry and Energy (MOTIE).

Conflict of Interest

The authors declare no conflict of interest.

Data Availability Statement

The data that support the findings of this study are available from the corresponding author upon reasonable request.

Keywords

electronic packaging, machine learning, MMIC, thermomechanical analysis

Received: September 8, 2022
Revised: October 24, 2022
Published online:

[1] J. Hasch, E. Topak, T. Zwick, R. Weigel, *IEEE Trans. Microwaves Theory Tech.* **2012**, *60*, 845.
[2] M. Hitzler, S. Saulig, L. Boehm, W. Mayer, W. Winkler, N. Uddin, C. Waldschmidt, *IEEE Trans. Microwaves Theory Tech.* **2017**, *65*, 1682.
[3] G. O. Arican, N. Akcam, E. Yazgan, *Microwaves Opt. Technol. Lett.* **2021**, *63*, 417.
[4] S.-H. Li, S. S. H. Hsu, J. Zhang, K.-C. Huang, *IEEE Trans. Microwaves Theory Tech.* **2018**, *66*, 5676.
[5] U. K. Mishra, L. Shen, T. E. Kazior, Y.-F. Wu, *Proc. IEEE* **2008**, *96*, 287.
[6] H.-Q. Tao, W. Hong, B. Zhang, X.-M. Yu, *IEEE Microwaves Wirel Compon. Lett.* **2017**, *27*, 73.
[7] R. S. Pengelly, S, M. Wood , J. W. Milligan, S. T. Sheppard, W. L. Pribble, *IEEE Trans. Microwaves Theory Tech.* **2012**, *60*, 1764.
[8] E. R. Heller, A. Crespo, *Miroelectron. Reliab.* **2008**, *48*, 45.
[9] T.-Y. Wu, Y. Tsukada, W. T. Chen, in *Proc. 46th Electron. Compon. Technol. Conf.*, IEEE, Piscataway, NJ **1996**, p. 524.
[10] A. Amar, B. Radi, A. E. Hami, *Miroelectron. Reliab.* **2021**, *124*, 114299.
[11] R. Zhang, W. S. Zhao, W. Y. Yin, *Miroelectron. Reliab.* **2014**, *54*, 575.
[12] J. P. Jones, E. Heller, D. Dorsey, S. Graham, *Miroelectron. Reliab.* **2015**, *55*, 2634.
[13] A. Prejs, S. Wood, R. Pengelly, W. Pribble, in *Proc. IEEE MTT-S Int. Microwaves Symp. Dig.*, IEEE, Piscataway, NJ **2009**, p. 917.
[14] L. Liang, M. Liu, C. Martin, W. Sun, *J. R. Soc. Interface* **2018**, *15*, 20170844.
[15] L. Liang, W. Mao, W. Sun, *J. Biomech.* **2020**, *99*, 109544.
[16] A. Balu, S. Nallagonda, F. Xu, A. Krishnamurthy, M.-C. Hsu, S. Sarkar, *Sci. Rep.* **2019**, *9*, 18560.
[17] X. Liu, C. E. Athanasiou, N. P. Padture, B. W. Sheldon, H. Gao, *Acta Mater.* **2020**, *190*, 105.
[18] Z. Nie, H. Jiang, L. B. Kara, *J. Comput. Inf. Sci. Eng.* **2020**, *20*, 011002.
[19] M. Mozaffer, R. Bostanabad, W. Chen, K. Ehmann, J. Cao, M. A. Bessa, *Proc. Natl. Acad. Sci. USA* **2019**, *116*, 26414.
[20] D.-W. Kim, J. H. Lim, S. Lee, *Composites, Part B* **2021**, *225*, 109314.
[21] W. Chu, P. S. Ho, W. Li, *IEEE Trans Compon. Packaging Manuf. Technol.* **2021**, *11*, 1435.
[22] S. W. Liu, S. K. Panigraphy, K. N. Chiang, in *Proc. IEEE 70th Electron. Compon. Technol. Conf.*, IEEE, Piscataway, NJ **2020**, p. 1626.
[23] M. Mao, W. Wang, C. Lu, F. Jia, X. Long, *Miroelectron. Reliab.* **2022**, *134*, 114553.
[24] P. H. Chou, H. Y. Hsiao, K. N. Chiang, in *Proc. IEEE 69th Electron. Compon. Technol. Conf.*, IEEE, Piscataway, NJ **2019**, p. 1515.
[25] C. C. A. Yuan, C.-C. Lee, *IEEE Access* **2020**, *8*, 143494.
[26] V. Samavatian, M. Fotuhi-Firuzabad, M. Samavatian, P. Dehghanian, F. Blaabjerg, *Sci. Rep.* **2020**, *10*, 14821.
[27] R. Guggenheim, L. Rodes, in *Proc. IEEE Int. Conf. Microw. Antennas Commun. Electron. Syst.*, IEEE, Piscataway, NJ **2017**, p. 1.
[28] A. R. Powell, L. B. Rowland, *Proc. IEEE* **2002**, *90*, 942.
[29] K. Kuang, R. Sturdivant, *RF and Microwave Microelectronics Packaging II*, Springer, New York **2017**.
[30] M. Faqir, T. Batten, T. Mrotzek, S. Knippscheer, M. Massiot, M. Buchta, H. Blanck, S. Rochette, O. Vendier, M. Kuball, *Miroelectron. Reliab.* **2012**, *52*, 3022.
[31] H. Oprins, V. O. Cherman, B. Vandevelde, G. Van der Plas, P. Marchal, E. Beyne, in *Proc. IEEE 62nd Electron. Compon. Technol. Conf.*, IEEE, Piscataway, NJ **2012**, p. 1081.
[32] R. Sturdivant, A. Bogdon, E. K. P. Chong, *J. Electron. Cool. Therm. Control* **2017**, *7*, 1.
[33] J. P. Calame, R. E. Myers, F. N. Wood, S. C. Binari, *IEEE Trans. Compon. Packag. Manuf. Technol.* **2005**, *28*, 797.
[34] K. Belkacemi, R. Hocine, *J. Low Power Electron. Appl.* **2018**, *8*, 23.
[35] D. A. Gajewski, S. Sheppard, T. McNulty, J. B. Barner, J. Milligan, J. Palmour, in *Proc. 26th Annual JEDEC ROCS Workshops*, Indian Wells, CA **2011**, p. 141.
[36] A. Landi, A. A. Mon, L. Liaci, A. Sitta, M. Calabretta, A. Sciuto, G. D. Arrigo, M. Renna, V. Vinciguerra, in *Proc. Int. Conf. Therm. Mech. Multi-Phys. Simul. Exp. Microelectron. Microsyst. (EuroSimE)*, IEEE, Piscataway, NJ **2021**, p. 1.
[37] M.-Y. Tsai, C. H. J. Hsu, C. T. O. Wang, *IEEE Trans. Compon. Packaging Manuf. Technol.* **2004**, *27*, 568.
[38] S. F. Popelar, in *Proc. 4th Int. Symp. Adv. Packag. Mater.*, IEEE, Piscataway, NJ **1998**, p. 41.

[39] M. K. Chengalva, in *Proc. Int. Soc. Conf. Thermal Phenomena*, IEEE, Piscataway, NJ **2002**, p. 876.
[40] P. O. Quintero, F. P. McCluskey, *IEEE Trans. Device Mater. Reliab.* **2011**, *11*, 531.
[41] W. D. van Driel, M. A. J. van Gils, R. B. R. van Silfhout, G. Q. Zhang, *Miroelectron. Reliab.* **2005**, *45*, 1633.
[42] C. H. Hsueh, C. R. Luttrell, S. Lee, T. C. Wu, H. Y. Lin, *J. Am. Ceram. Soc.* **2006**, *89*, 1632.
[43] E. A. Daoud, *Int. J. Comput., Inf., Syst. Sci., Eng.* **2019**, *13*, 6.
[44] G. Ke, Q. Meng, T. Finley, T. Wang, W. Chen, W. Ma, Q. Ye, T.-Y. Liu, *Adv. Neural Inf. Process Syst.* **2017**, *30*, 3149.
[45] H. Shi, *Master Thesis*, The University of Waikato **2007**.
[46] O. I. Abiodun, A. Jantan, A. E. Omolara, K. V. Dada, N. A. Mohamed, H. Arshad, *Heliyon* **2018**, *4*, e00938.
[47] J. V. Tu, *J. Clin. Epidemiol.* **1996**, *49*, 1225.
[48] DMLC. xgboost. https://github.com/dmlc/xgboost (accessed: May 2022).
[49] Microsoft. LightGBM, https://github.com/microsoft/LightGBM (accessed: May 2022).
[50] M. Abadi, P. Barham, J. Chen, Z. Chen, A. Davis, J. Dean, M. Devin, S. Ghemawat, G. Irving, M. Isard, M. Kudlur, J. Levenberg, R. Monga, S. Moore, D. G. Murray, B. Steiner, P. Tucker, V. Vasudevan, P. Warden, M. Wicke, Y. Yu, X. Zheng, *Proc. OSDI* **2016**, *16*, 265.